Influence of orientation on the contrast of high-angle annular dark-field images of silicon

Dmitri O. Klenov*
Materials Department, University of California, Santa Barbara, California 93106-5050, USA

Scott D. Findlay and Leslie J. Allen
School of Physics, The University of Melbourne, Victoria 3010, Australia

Susanne Stemmer†
Materials Department, University of California, Santa Barbara, California 93106-5050, USA
(Received 5 April 2007; published 18 July 2007)

Atom column intensities of silicon single crystals oriented along different crystallographic orientations are compared in experimental and simulated high-angle annular dark-field images in scanning transmission electron microscopy. The intensity of a background, measured between the columns, is also evaluated and found to be largely independent of the column spacing. The contrast is lower in the experiments, and it has been suggested previously that this follows because the background is higher in the experiments. We explore the extent to which the comparison of experimental atom column intensities with image simulations is aided by subtraction of the background for these data. We also explore an alternative view: simple simulations overestimate the contrast because spatial incoherence and associated instabilities are not taken into account. The results do not distinguish between these approaches, which need not be in opposition, and we describe experiments which might further clarify matters.

DOI: 10.1103/PhysRevB.76.014111 PACS number(s): 68.37.Lp, 61.14.−x

INTRODUCTION

The contrast of high-angle annular dark-field (HAADF) images obtained in scanning transmission electron microscopy (STEM) of crystalline materials is known to be sensitive to the average atomic number of the species occupying the atomic columns.[1,2] A quantitative understanding of HAADF image contrast would allow for the identification of the type and number of species in a column. Significant progress has been made in the simulation of HAADF images, incorporating both high-angle elastic and thermal diffuse scattering.[3–9]

Two of the present authors (Klenov and Stemmer) recently studied the influence of sample thickness and other imaging parameters on atom column intensities of experimental HAADF images of $PbTiO_3$, $SrTiO_3$, and InP.[10,11] While no contrast reversals were observed up to ~400 nm, the experimental contrast is much less than predicted in simulations. In that work, it was found that comparison between experiment and multislice image simulations[12] was greatly improved if a "background" intensity (measured between the columns) was subtracted, if comparisons were made only between minimum and maximum values in each image. Similar favorable comparisons using this approach have been made previously.[13] This background was found to rapidly increase with thickness. It scaled with the average atomic number of the crystal and was not adequately reproduced in multislice image simulations without thermal diffuse scattering.[10] Possible origins for a high background intensity in the experiments not accounted for in the image simulations included point defects, surface layers or strains, and inelastic and/or multiple elastic/inelastic scattering.

However, other effects in the electron microscope, most notably instrumental and environmental effects such as the finite source size and instabilities, can also reduce the contrast. In the parlance of Ref. 10, these effects serve not to increase the background but rather to reduce the signal above the background.

In the present study, we keep the probe and environmental factors constant while varying the column spacing. This is achieved by investigating the HAADF image contrast of silicon single crystals along different orientations. Analyzing the image contrast within one material (silicon) also allows for reliable comparisons of contrast as a function of sample thicknesses, as estimates of the thickness obtained from low-loss electron energy-loss spectroscopy (EELS) should have similar systematic errors.

The experimental data are compared with simulations. Because silicon is a relatively light matrix, measurements have been collected out to large thicknesses so that trends in the data are clear. Large thicknesses are a hindrance to the frozen phonon method of simulation,[12,14] which scales linearly with thickness. Therefore comparisons are primarily made with Bloch wave simulations based on the mixed dynamic form factor formalism.[9] The shortcomings of this approach and the improvements the frozen phonon model may provide are discussed.

We explore both approaches: that of subtracting the background and that of reducing the contrast through the inclusion of source incoherence. The results do not distinguish between these views, and indeed, both effects may contribute simultaneously. We briefly outline further experiments that might help to distinguish between the different contributing factors to the discrepancy in contrast.

EXPERIMENT

Cross-section STEM samples were prepared by gluing together three different orientations of a silicon wafer for viewing along [110], [100], and [112] within one stack. For comparison, a second sample was also investigated along [110]

to ensure reproducibility. The samples were prepared by conventional polishing followed by argon ion milling (Gatan Precision Ion Polishing System) at 3 kV and plasma cleaning prior to insertion into the microscope. Images were recorded using a field-emission transmission electron microscope (Tecnai F30UT) operated at 300 kV with UltraTwin lens ($C_s \sim 0.52$ mm). The convergence semiangle was ~10.1 mrad. The HAADF detector (Fischione) inner and outer radii were 68 and 476 mrad, respectively. Other characteristics of this microscope, including probe size and shape, have been reported previously.[10,11]

HAADF images were recorded using identical experimental conditions (1024×1024 images, acquisition time: 50 s, magnification: 10.6 pm/pixel, and fixed brightness/contrast settings) to allow for direct comparison of measured image intensities. Images along different zone axes were recorded in the same session using the focus that provided the maximum column intensities.[10]

The transmission electron microscope (TEM) foil thickness was estimated from low-loss EELS. For each image in a series, an EELS spectrum was recorded using a collection semiangle of 18.3 mrad. The ratio of the thickness t to the total mean free path length λ was calculated from $\ln(I_t/I_0)$, where I_t was the total area under the spectrum and I_0 the area under the zero loss peak,[15] extracted using the Gatan software (DIGITALMICROGRAPH). The maximum thicknesses reported here were limited by the ability to extract the zero loss peak ($t/\lambda \sim 5$) and not by the contrast of atomic columns in the images. Measured t/λ ratios were converted to thicknesses by estimating λ (~131 nm), as described by Egerton.[15]

The intensity of the silicon atom columns (or dumbbells, where columns were not resolved) I_{tot} and the background intensity I_B (measured between the columns) were obtained from histograms of the entire image for each thickness. Thus measured column intensities were obtained from all fringes in each image. In addition, a background subtracted column intensity $I_S = I_{tot} - I_B$ was obtained. The spatial resolution was insufficient to resolve the silicon dumbbells along [112]. The dumbbells along [110] were not visible in all images, due to the relatively long exposure times chosen to reduce the noise in the intensities, although they were resolved for shorter acquisition times. A small drift was present in many images because waiting for the stage to stabilize after moving to a different thickness was not practical. The drift did not impact intensity values obtained from the histograms. All images were as-recorded and no filtering or other image processing was performed. The dark level was measured in the hole in the sample.[16]

Figure 1 shows selected HAADF-STEM images recorded from the different sample thicknesses along three different zone axes, [100], [110], and [112], respectively. Atomic structure images are observed even for the largest thicknesses, consistent with earlier reports for silicon.[17] The main change with increasing thickness is an increase in the noise level, caused by the increase in background, as discussed below.

SIMULATION

HAADF image simulations were initially carried out in a Bloch wave model, based on the mixed dynamical form factor approach, as described in Ref. 9. The defocus value appropriate for the simulations was determined in analogy with the experimental procedure: defocus values were scanned through to determine the value at which the signal peaks. A plot of the signal strength as a function of both defocus value and specimen thickness is shown in Fig. 2 for the [110] orientation of silicon. The defocus value at which the signal peaks varies as a function of thickness, beginning at −26 nm, decreasing to −30 nm, and increasing again to tend toward a steady −25 nm in the large thickness limit. Similar behavior occurs in the other orientations. For all subsequent simulations, for all orientations, the defocus was taken to be −27 nm. The breadth of the peak along the defocus axis in Fig. 2 and simulations, not shown here, of the contrast of pertinent HAADF images suggest that using this single value as a compromise is acceptable.

For each orientation, line scans were simulated along the significant axis (across the dumbbells in [110] and [112] orientations), and the maximum and minimum values were taken to represent I_{tot} and I_B. This Bloch wave approach

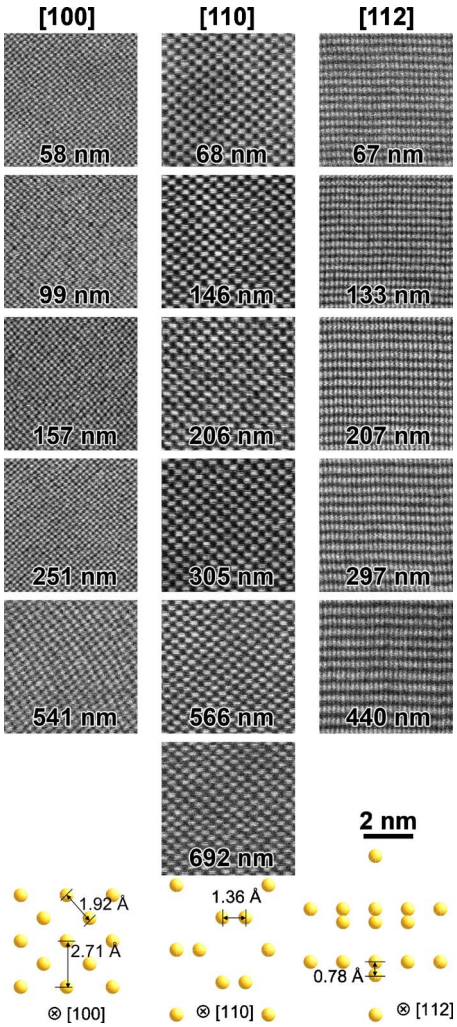

FIG. 1. (Color online) Selected HAADF images from a thickness series along [100], [110], and [112] in silicon. The dumbbells along [110] are not always clearly resolved due to the relatively long acquisition time. The bottom row shows a projection of the unit cell along each direction and selected projected distances.

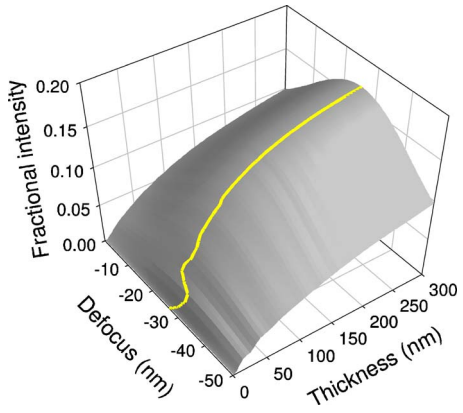

FIG. 2. (Color online) Simulations for the intensity with the probe atop a column of silicon viewed along the [110] axis as a function of specimen thickness and defocus. The line traced on the surface shows the location of the maximum signal strength at each thickness value.

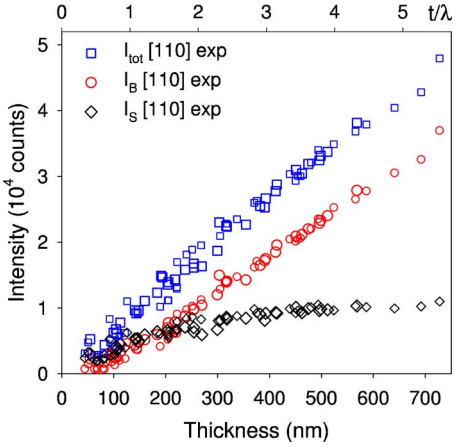

FIG. 3. (Color online) Experimental image intensities I_{tot}, I_B, and I_S along [110] as a function of thickness. The experimental t/λ ratios used to estimate the thickness are shown on the top horizontal axis. The data were obtained from two different samples, as indicated by the different symbol size.

allows for multiple elastic scattering prior to a thermal scattering event, but does not account for further elastic or inelastic scattering of the thermally scattered electrons. As such, the total signal saturates as the thickness increases and the number of electrons remaining in the elastic wave function dwindles. This is a shortcoming of the model. In practice, multiple thermal scattering events, which become increasingly likely with increasing thickness, tend to shift the distribution of thermally scattered electrons to increasingly large angles. For the annular detector used, with moderately large inner angle and very large outer angle, the increase in signal with sample thickness will most likely be greater than predicted in the single elastic-to-inelastic scattering model.

The frozen phonon model should, in principle, overcome these difficulties. However, several practicalities make it difficult to apply here. The maximum sample thickness considered is very large, and so the real space cell size should be large to accommodate the spreading of the probe with increasing thickness. The detector spans a large range, and so the reciprocal space cell size should be very large. The parameters here are such that these conditions cannot both be satisfied with tractable array sizes. Furthermore, the large thickness makes the calculations, which scale linearly with thickness, very slow, especially if several probe positions are required. Simulations of zone axis images for 600 nm samples are a nonstarter. Nevertheless, in violation of some of the conditions for fully converged frozen phonon simulations, we shall show some simulations for a 68–240 mrad detector, to give an indication of the difference in behavior expected between the Bloch wave and frozen phonon model approaches.

UNDERESTIMATING THE BACKGROUND

Figure 3 shows experimental image intensities I_{tot}, I_B, and I_S along [110] as a function of thickness. I_{tot} and I_B increase with thickness. The increase in I_B is less rapid than for $SrTiO_3$ and $PbTiO_3$ as reported previously,[10] consistent with the lower atomic number of silicon. I_S saturates at thicknesses greater than ~300 nm. By definition, I_B contributes to the intensity both between and on the atomic columns so that I_S, and not I_{tot}, represents the atomically resolved contrast. At a critical distance from the entrance surface, the probe becomes wider than the atomic column on which it was initially focused[18] and I_S ceases to increase. Any further increase in I_{tot} with thickness merely reflects the increase in I_B, i.e., scattering from the surrounding crystal, and does not contribute to atomic structure information in the images. Despite the uncertainty in the thickness estimates from EELS, the results show that the critical thickness (~300 nm) is larger in silicon than $SrTiO_3$ or $PbTiO_3$, where it was about 60–100 nm.[10]

Figure 4 compares the measured and simulated intensities I_{tot}, I_B, and I_S as a function of thickness (and experimental t/λ) for the three different silicon orientations. Since Ref. 10 found the best agreement between the experimental and simulated values of I_S, the simulations have been normalized against the experimental data by fixing the large thickness results of the I_S plots for good visual agreement. This assumption strongly influences the conclusions drawn about any discrepancies between simulation and experiment, a point we shall return to in the next section.

Within the experimental error, the measured I_{tot} [Fig. 4(a)] are similar for all orientations and increase nearly linearly with thickness. The difference in the simulated I_{tot} for the different directions is relatively small. The simulated I_{tot} saturates at larger thicknesses.

The measured I_B [Fig. 4(b)] is very similar for the different orientations, consistent with the simulations. The background intensity I_B is, however, much higher in the experiments [Figs. 3 and 4(b)] than in the simulations [Fig. 4(b)], in particular, at large thicknesses. For example, along [110] the experimental I_B exceeded 50% of I_{tot} at thicknesses $>\sim 200$ nm (Fig. 3), whereas the calculated I_B remains below 50% of I_{tot} for all thicknesses [Figs. 4(a) and 4(b)]. The saturation observed in the simulated but not in the experimental I_{tot} could thus be explained with the smaller simu-

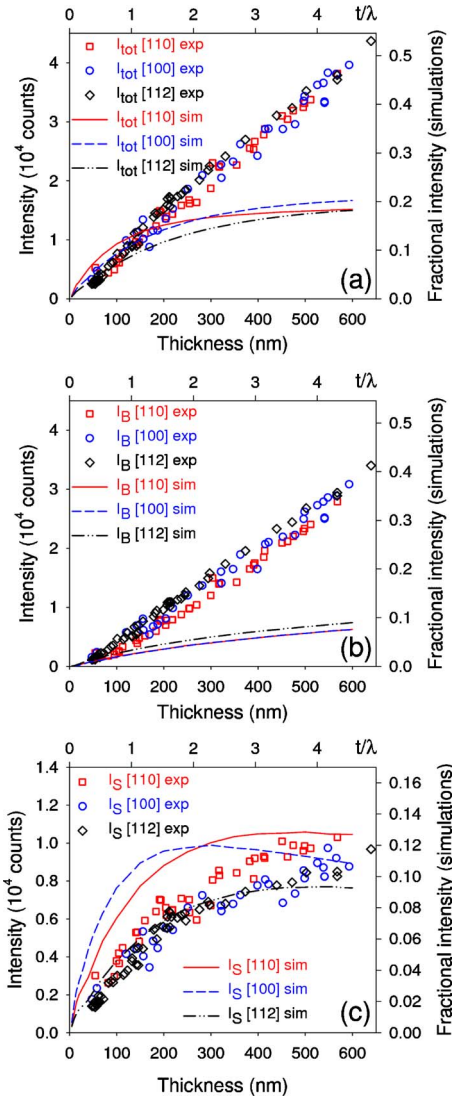

FIG. 4. (Color online) Experimental and simulated image intensities (a) I_{tot}, (b) I_B, and (c) I_S along the three different directions as a function of thickness. The experimental t/λ ratios that were used to estimate the thickness are shown on the top horizontal axis. Note the different vertical axes ranges in (c).

lated I_B. The higher I_B in the experiments is consistent with what was previously observed for $SrTiO_3$ and $PbTiO_3$ and multislice image simulations.[10]

Figure 4(c) shows the atom column intensities I_S after subtraction of the background. Both simulated and experimental I_S saturate at thickness larger than 200–300 nm for all orientations. While the experimental I_S is similar for all orientations, simulations predict a lower intensity for [112], as would be expected based on the larger spacing of atoms along this direction. Both simulations and experiments show a higher I_S along [110]. At least some of the differences between experiments and simulations are likely due to deviations from the "maximum contrast" focus in the experiments. Focusing is easier along [110], as resolving the dumbbells provides for an additional focusing criterion. Another explanation for differences between simulations and experiments is errors in the thickness estimates. For example, ion-milled samples are likely to have amorphous surface layers not present in simulations, and estimates of the total inelastic mean free path length contain significant errors. As both effects likely result in an overestimation of the sample thickness, the agreement between simulated and experimental I_S is probably better than apparent from Fig. 4(c). However, thickness errors are not expected to be large enough to affect any of the conclusions drawn in the following.

To this point, it would appear that the simulations are woefully underestimating the background contribution I_B. Perhaps other inelastic processes that are not being taken into account play a role. The thickness determination procedure puts the maximum thickness at $t/\lambda \sim 5$, which corresponds to only 1% of the recorded spectrum being in the zero loss peak. It may well be that simulations which assume that all electrons are either in the elastic wave function or have undergone thermal diffuse scattering are unsuited to model such a case. However, the conclusion that the background is overestimated follows from the assumption that the scaled I_S is well described by simulation. What if I_S is being significantly overestimated?

OVERESTIMATING THE SIGNAL

That the size of the background is very similar for the different orientations in which the column spacing is notably different has been presented as evidence against the idea that the lack of contrast is probe dependent, say, through incoherence in the source. Perhaps it would be better to say that it counts against it being the sole influence. However, some spatial incoherence (finite extent of the effective illumination source) would serve to reduce the contrast. Spatial incoherence in STEM is modeled by convolving simulated STEM images by a spread function describing the effective source,[19] usually taken to be a Gaussian. (There is no *a priori* reason for assuming the effective source to have a Gaussian distribution. The ramifications that other distributions may have are largely unexplored. We are grateful to Dwyer for this observation.) Figure 5 shows the effects of spatial incoherence on the values of I_{tot}, I_B, and I_S for a few select effective source sizes characterized by their Gaussian half width at half maximum (HWHM) for the [110] zone axis. As expected, the blurring serves to reduce the contrast, bringing I_{tot} and I_B closer together and so reducing I_S. Simulations for the [100] and [112] zone axes, not shown here, show that the amount of blurring required for I_S to drop below I_B varies somewhat for the different orientations, with the [110] orientation requiring the most blurring to bring about that change. Given the similarity in the experimental data, this may count against spatial incoherence providing the sole explanation for the discrepancy.

Both I_{tot} and I_B show almost linear increase in intensity with thickness for the larger thickness values explored. The simulations saturate in the middle of the range shown and so do not display this behavior. This difference in trend, let alone scale, could be suggestive of the nature of the additional background, but is more probably a limitation of the model based on absorption and a single elastic-to-inelastic scattering approach to the thermal scattering. The frozen

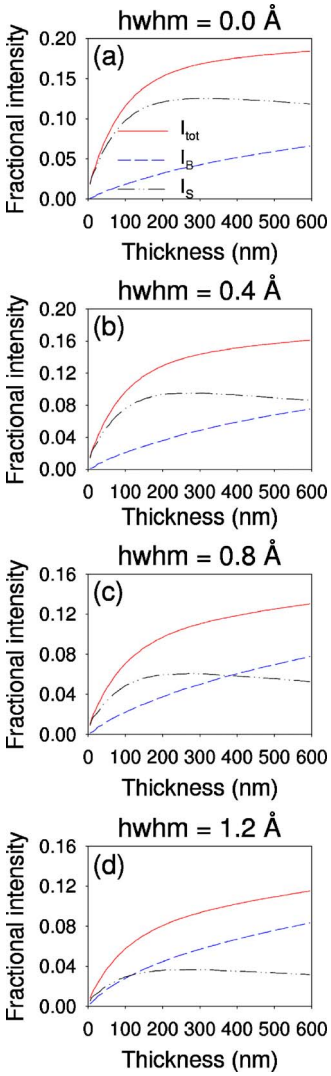

FIG. 5. (Color online) Bloch wave simulations showing I_{tot}, I_B, and I_S for the [110] zone axis orientation for different effective source sizes as characterized by the half-width at half maximum (HWHM) of the Gaussian used in the convolution.

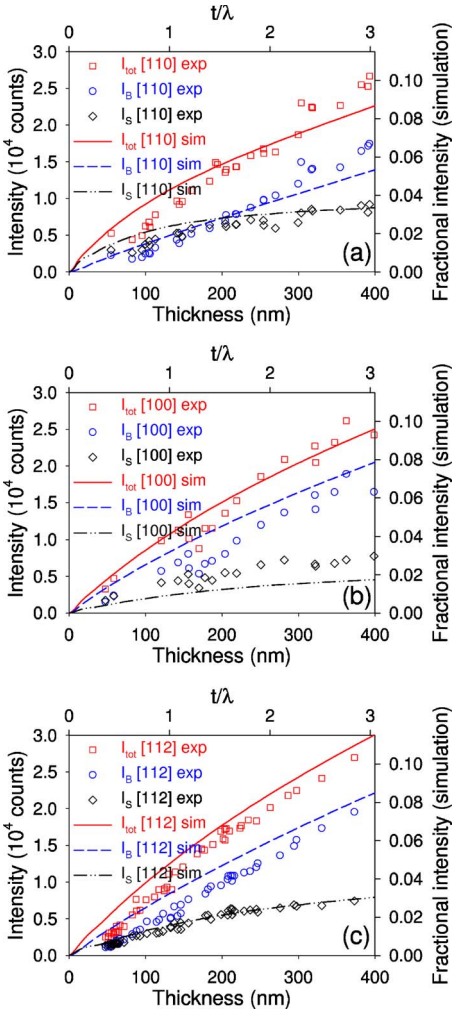

FIG. 6. (Color online) Comparison of the experimental data with results of a rudimentary frozen phonon simulation where a blurring with a Gaussian of 1.0 Å half-width at half maximum has been applied.

phonon model should, in principle, overcome these difficulties. However, as mentioned earlier, performing converged frozen phonon calculations for the current parameters is very computationally demanding, particularly if a full zone axis image must be calculated in order to simulate the effect of spatial incoherence. Nevertheless, we have carried out rudimentary frozen phonon simulations as follows. We use only a single pass per probe position, and take advantage of symmetry and smoothness to calculate only for a modest number of probe positions, interpolating to a fuller image which is then convolved with a Gaussian to model spatial incoherence. The HAADF detector is taken to span only 68–240 mrad, smaller than that used in the experiment, though the qualitative similarity between Bloch wave simulations for the two different detector sizes suggests that this should not prevent us drawing meaningful conclusions. Perhaps the most serious potential flaw of the calculation is that despite the 1024×1024 pixel array used, the wave function in real space wraps around beyond 100 nm or so. Whether this adversely affects the results is unclear. By the time the probe is this dispersed, the real space features which contribute to high-angle scattering are peakiness on individual columns, and this still happens after wraparound. Figure 6 shows the comparison between these frozen phonon calculations, assuming an effective source size with Gaussian half-width at half maximum of 1.0 Å, and the experimental data (note that the calculations only extend to 400 nm). Global scaling has been done across all three orientations to give the best visual fit.

The frozen phonon results for I_{tot} and I_B evince the linear behavior of the experimental data more than the Bloch wave results did. As such, the linear behavior of the experimental data should not be considered anomalous: it appears that the increase in signal due to multiple thermal scattering events at large sample thicknesses would push the simulations in this direction.

The first and second columns in Fig. 7 (simulated with a Bloch wave model assuming 400 nm thick specimens) compare the full HAADF images with no spatial incoherence to those assuming the 1.0 Å effective source. Comparison be-

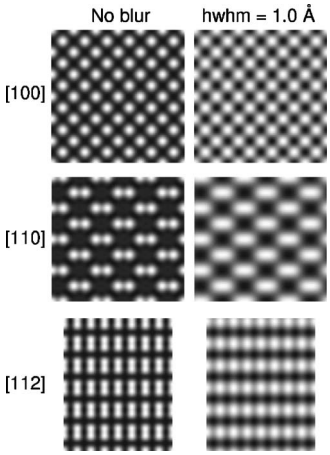

FIG. 7. Bloch wave simulations of the zone axis HAADF images for the three orientations for 400 nm thick specimens are shown with no blurring (first column) and after blurring with a Gaussian of 1.0 Å half-width at half maximum (second column).

tween the appearance of these images and those in Fig. 1 lend further support to the idea that simulations without some blurring do not correspond to what is observed in the experiments.

The comparison between these simulations and the data is quite favorable, though the effective source size used may seem quite large. As seen in Fig. 7, the 1.0 Å effective source size prevents resolution of the dumbbells in the [110] orientation. As noted earlier, while these dumbbells were not visible in most images, this is due to the relatively long exposure times used in order to reduce the noise in the recorded intensity. The microscope is easily capable of resolving dumbbells along ⟨110⟩ once the stage has stabilized if shorter recording times are used. The 1.0 Å effective source size cannot be solely due to spatial incoherence from the electron source then, but must rather also take into account some random jitter of the probe position relative to the specimen during the recording period.

DISCUSSION AND CONCLUSIONS

To try to distinguish among the many possible causes of the discrepancies seen previously between the contrast of simulated and experimental STEM images, additional experiments and comprehensive image simulations are required. Several approaches may be pursued to separate instrumental and environmental effects from genuine sample effects, such as varying the probe size, shape, or instabilities. In the present work, three different orientations in silicon were used, thus keeping the probe and environmental factors constant while varying the column spacing.

Consistent with previous observations,[10] experiments and simulations of atomic column intensities are in reasonable agreement after subtraction of a background that was much higher than in the experiments. The qualitative agreement in I_S between experiments and theory provides additional support that the previously developed approach of background subtraction is appropriate for quantifying contrast in HAADF images containing columns containing different species. In contrast to conventional high-resolution TEM ("Stobbs factor"[20,21]), experimental intensity ratios of different atomic columns calculated from I_S matched the scaled simulated contrast reasonably well after background subtraction.[10]

Within this conceptual framework, the results suggest that the background represents a genuine sample effect, rather than an instrumental or environmental effect. The background intensity measured from the histograms corresponded to the lowest intensity in the images. The largest projected column spacing in the image plane occurs along [110] (~0.41 nm) and the smallest along [100] (~0.27 nm), but the measured background intensities are similar along all zone axes, suggesting that the ratio of column distances to the fixed probe size (or to the amplitude of instabilities) does not affect the background intensity. This could indicate that the delocalized background signal is indeed characteristic for the scattering physics of the sample (small differences in the background as may be expected from the anisotropy in inelastic scattering[22] are either within the noise of the experimental data or did not affect the images). It is important to note that for probe sizes comparable to the column distances, i.e., larger than the ones employed here, it is expected that the background will depend on the column distances.[16]

Concerning the physics of high-angle scattering that could be responsible for a larger experimental background, multiple elastic-inelastic, inelastic (such as Compton scattering), or multiple inelastic scattering events are possible candidates.[23,24] Furthermore, real TEM samples may contain point defects that could contribute to additional delocalized scattering not present in the simulations of perfect samples.[20,21]

Background subtraction is a straightforward procedure for bulk crystals, though it is more difficult at interfaces and defects, where the background and its delocalization are less well defined.[10] As such, it could be suggested that experimental and simulated column intensities should only be compared after background subtraction, and to some extent, this may be a helpful approach. However, it is conceptually unsatisfying in many respects. Most notably, the size of the background relative to the signal is so large that if the background indicates some process not included in current simulations, then it is unclear why the simulations should be sufficiently sound as to provide an accurate model for the remaining signal component.

The alternative view explored in this paper is that routine simulations significantly overestimate the signal because they do not take into account effects such as spatial incoherence (finite source size in STEM and mechanical instabilities). We have shown that including finite effective source size via a convolution with a Gaussian distribution significantly improves the comparison between the simulated and experimental values of I_{tot}, I_B, and I_S. That all values can be simultaneously modeled, without invoking anything beyond what is well understood, is very attractive. However, preliminary simulations suggest that spatial incoherence alone would not explain the $PbTiO_3$ and $SrTiO_3$ presented previously.[10,11] In particular, blurring tends to suppress the TiO column in $PbTiO_3$ into the background, which was not seen in the experiment. Nevertheless, it seems likely, particu-

larly from the comparison in Fig. 7, that spatial incoherence or some similar effect always plays some role.

The first approach posited the presence of a large background which is not very well understood. The second asserted that the contrast mismatch was due to neglecting such effects as spatial incoherence. The present experiments do not rule out either possibility. While the reality may involve a mix of the two, individually their predictions are sufficiently different that experiments can be suggested which would distinguish the two cases. Simulations give the recorded intensity (current) as a fraction of the incident intensity (current). The latter is seldom known experimentally, but absolute values would go a long way toward distinguishing an anomalous additional background on top of the contribution given by standard simulations and the case where the effective signal is reduced due to finite source size and microscope instabilities. If the signal is correctly modeled by simulation, then comparison of Figs. 3 and 4(c) suggests that by 400 nm 10% of the incident current is in I_S, 40% is in I_B, and thus, 50% is in I_{tot}. Conversely, if spatial incoherence is largely to blame, then analysis of Fig. 6 suggests that I_{tot} comprises only 10% of the incident current, with I_S accounting for only a few percent.

Energy filtered HAADF images might help,[25] particularly if the background is to be attributed to inelastic scattering processes other than thermal diffuse scattering (though it is hard to envisage what other processes would lead to such high-angle scattering). An independent measure of the effective source size which could then be compared to that used here, essentially taken as a fitting parameter, would also be very instructive.

It should be emphasized that the background intensity in experiments is substantial even for a very light element such as silicon, and drastically increases with thickness and average atomic number.[10] Despite the uncertainties in the thickness measurements and the noise in the experimental data, the measured and simulated I_{tot} show fundamentally different behaviors as a function of thickness. Simulated and experimental I_{tot} might still agree reasonably for a light element such as silicon and typical sample thicknesses that are less than 100 nm.[22] However, for samples containing heavier elements, such as $SrTiO_3$,[10,11] some further insight is required if qualitative and quantitative comparisons are to be undertaken even for the thinnest specimens.

ACKNOWLEDGMENTS

S.S. and D.O.K. thank the DOE Office of Basic Energy Sciences for support (Grant DE-FG02-06ER45994). L.J.A. acknowledges support from the Australian Research Council. L.J.A. and S.D.F. thank C. Dwyer and P. D. Nellist for helpful discussions.

*Present address: FEI Company, Achtseweg Noord 5, 5651 GG Eindhoven/Acht, The Netherlands.
†stemmer@mrl.ucsb.edu

[1] J. C. H. Spence, *High-Resolution Transmission Electron Microscopy*, 3rd ed. (Oxford University Press, Oxford, 2003).
[2] S. J. Pennycook and D. E. Jesson, Ultramicroscopy **37**, 14 (1991).
[3] E. J. Kirkland, R. F. Loane, and J. Silcox, Ultramicroscopy **23**, 77 (1987).
[4] P. R. Xu, R. F. Loane, and J. Silcox, Ultramicroscopy **38**, 127 (1991).
[5] S. Hillyard and J. Silcox, Ultramicroscopy **58**, 6 (1995).
[6] P. D. Nellist and S. J. Pennycook, Ultramicroscopy **78**, 111 (1999).
[7] K. Watanabe, T. Yamazaki, I. Hashimoto, and M. Shiojiri, Phys. Rev. B **64**, 115432 (2001).
[8] K. Ishizuka, J. Electron Microsc. **50**, 291 (2001).
[9] L. J. Allen, S. D. Findlay, M. P. Oxley, and C. J. Rossouw, Ultramicroscopy **96**, 47 (2003).
[10] D. O. Klenov and S. Stemmer, Ultramicroscopy **106**, 889 (2006).
[11] D. O. Klenov and S. Stemmer, Jpn. J. Appl. Phys., Part 2 **45**, L602 (2006).
[12] E. J. Kirkland, *Advanced Computing in Electron Microscopy* (Plenum, New York, 1998).
[13] K. Watanabe, T. Yamazaki, Y. Kikuchi, Y. Kotaka, M. Kawasaki, I. Hashimoto, and M. Shiojiri, Phys. Rev. B **63**, 085316 (2001).
[14] R. F. Loane, P. R. Xu, and J. Silcox, Acta Crystallogr., Sect. A: Found. Crystallogr. **47**, 267 (1991).
[15] R. F. Egerton, *Electron Energy-Loss Spectroscopy in the Electron Microscope*, 2nd ed. (Plenum, New York, 1996).
[16] Z. H. Yu, P. E. Batson, and J. Silcox, Ultramicroscopy **96**, 275 (2003).
[17] A. C. Diebold, B. Foran, C. Kisielowski, D. A. Muller, S. J. Pennycook, E. Principe, and S. Stemmer, Microsc. Microanal. **9**, 493 (2003).
[18] S. Hillyard, R. F. Loane, and J. Silcox, Ultramicroscopy **49**, 14 (1993).
[19] P. D. Nellist and J. M. Rodenburg, Ultramicroscopy **54**, 61 (1994).
[20] M. J. Hÿtch and W. M. Stobbs, Ultramicroscopy **53**, 191 (1994).
[21] A. Howie, Ultramicroscopy **98**, 73 (2004).
[22] P. E. Batson, Ultramicroscopy **106**, 1104 (2006).
[23] A. L. Bleloch, M. R. Castell, A. Howie, and C. A. Walsh, Ultramicroscopy **54**, 107 (1994).
[24] C. B. Boothroyd, R. E. Dunin-Borkowski, and T. Walther, in *Atomic Resolution Microscopy of Surfaces and Interfaces*, edited by D. J. Smith (Materials Research Society, Pittsburgh, 1997), Vol. 466, p. 113.
[25] T. Walther, J. Microsc. **221**, 137 (2006).